

## RESEARCH ARTICLE

10.1029/2017JD027952

## Key Points:

- PM<sub>10</sub>, PM<sub>2.5</sub>, and PM<sub>1</sub> were collected in Guangzhou in summer 2013 for measurements of carbonaceous aerosols, ions, and tracers
- <sup>14</sup>C results showed that 87% of EC and 53% of OC in PM<sub>2.5</sub> were derived from fossil sources on a typical summer day
- Nonfossil sources from rural and suburban areas triggered the haze formation

## Supporting Information:

- Supporting information S1

## Correspondence to:

J. Li,  
junli@gig.ac.cn

## Citation:

Liu, J., Ding, P., Zong, Z., Li, J., Tian, C., Chen, W., et al. (2018). Evidence of rural and suburban sources of urban haze formation in China: A case study from the Pearl River Delta region. *Journal of Geophysical Research: Atmospheres*, 123, 4712–4726. <https://doi.org/10.1029/2017JD027952>




Received 2 NOV 2017

Accepted 5 APR 2018

Accepted article online 23 APR 2018

Published online 6 MAY 2018

## Evidence of Rural and Suburban Sources of Urban Haze Formation in China: A Case Study From the Pearl River Delta Region

Junwen Liu<sup>1,2,3</sup>, Ping Ding<sup>1</sup>, Zheng Zong<sup>4</sup>, Jun Li<sup>1</sup> , Chongguo Tian<sup>4</sup> , Weihua Chen<sup>5</sup>, Ming Chang<sup>3</sup>, Gary Salazar<sup>2</sup>, Chengde Shen<sup>1</sup>, Zhineng Cheng<sup>1</sup>, Yingjun Chen<sup>6</sup>, Xuemei Wang<sup>3</sup> , Sönke Szidat<sup>2</sup> , and Gan Zhang<sup>1</sup>

<sup>1</sup>State Key Laboratory of Organic Geochemistry and State Key Laboratory of Isotope Geochemistry, Guangzhou Institute of Geochemistry, Chinese Academy of Sciences, Guangzhou, China, <sup>2</sup>Department of Chemistry and Biochemistry and Oeschger Centre for Climate Change Research, University of Bern, Berne, Switzerland, <sup>3</sup>Institute for Environmental and Climate Research, Jinan University, Guangzhou, China, <sup>4</sup>Yantai Institute of Coastal Zone Research, Chinese Academy of Sciences, Yantai, China, <sup>5</sup>School of Environmental Science and Engineering, Sun Yat-sen University, Guangzhou, China, <sup>6</sup>College of Environmental Science and Engineering, Tongji University, Shanghai, China

**Abstract** Although particulate matter (PM)-driven haze is a common phenomenon in many Chinese cities, studies on the sources of its key components, such as organic carbon (OC) and elemental carbon (EC), are poorly constrained. In this study, PM with aerodynamic diameters less than 10 (PM<sub>10</sub>), 2.5 (PM<sub>2.5</sub>), and 1 μm (PM<sub>1</sub>) were collected at an urban site in the core city of the Pearl River Delta region in summer 2013. The average PM<sub>10</sub>, PM<sub>2.5</sub>, and PM<sub>1</sub> mass concentrations were 109 ± 28.4, 57.7 ± 15.0, and 50.9 ± 13.2 μg/m<sup>3</sup>, respectively. A PM-driven haze bloom-decay process was observed from 9 to 14 July and studied based on radiocarbon (<sup>14</sup>C) and stable nitrogen isotope (<sup>15</sup>N). The <sup>14</sup>C results revealed that 87% of EC and 53% of OC in PM<sub>2.5</sub> were derived from fossil sources on a typical summer day (9 July), while these values fell to 79% and 40% on 12 July and 76% and 29% on 13 July, respectively, due to the invasion of nonfossil-enriched air masses from rural/suburban areas. In addition, a <sup>15</sup>N-derived model showed that nonfossil sources contributed 5% of NH<sub>3</sub> on 9 July, which increased to about 80% on 12 and 13 July. However, the <sup>15</sup>N-NO<sub>3</sub><sup>−</sup> values were relatively stable, probably because of the large area of overlap in <sup>15</sup>N-NO<sub>x</sub> from biomass burning and traffic exhaust. To our knowledge, this work is the first study to report both daily <sup>14</sup>C and <sup>15</sup>N signals in China and identify nonfossil sources from rural/suburban areas as triggers of summer haze.

## 1. Introduction

Particulate matter (PM), generally classified as PM<sub>10</sub> (≤10 μm), PM<sub>2.5</sub> (≤2.5 μm), and PM<sub>1</sub> (≤1 μm) based on the aerodynamic diameter, is derived from both natural and anthropogenic activities and has profound impacts on air quality, climate system, and human health. Concretely speaking, high PM concentration could significantly lower atmospheric visibility (Y. Liu, Zhang, et al., 2014), cause huge numbers of people died earlier (Lelieveld et al., 2015), and has the potential to trigger regional floods or droughts by modifying the balance of atmospheric circulation (Fan et al., 2015; Menon et al., 2002). Therefore, atmospheric PM has been a major topic of interest of scientific research for decades.

China has the second largest economy and is the most populous country in the world and is challenged with high PM loadings and severe haze pollution. Numerous investigations have examined PM chemical compositions, emission sources, optical properties, and atmospheric processes in China (Cao et al., 2004, 2007; Cheng et al., 2013; Duan et al., 2004; Han et al., 2016; Sun et al., 2014, 2016; Yan et al., 2015; Yang et al., 2016; M. Zheng et al., 2005). However, most studies have focused on only one PM size fraction and have focused mainly on northern regions of China, such as the Beijing-Tianjin-Hebei urban agglomeration, where severe air pollution frequently occurs. Few studies have examined other heavily polluted areas or emphasized the haze formation process (Guo et al., 2014; Sun et al., 2014) or daily dynamic changes (J. Liu, Li, Liu, et al., 2016), limiting our understanding of the impact of emission sources on the chemical composition, formation, and evolution of haze pollution.

Guangzhou, located in the Pearl River Delta (PRD) urban agglomeration, is the largest city in South China, with a land area of ~7,500 km<sup>2</sup> and a population of ~13 million. The most important contributors of PM<sub>10</sub> in

Guangzhou during the 2004 summer season were traffic exhaust (33–43%) and coal combustion (20–32%), as evidenced by a multivariate linearly regression analysis (X. Wang, Bi, et al., 2006). Combining aerosol mass spectrometry and source-specific tracers, Huang et al. (2014) found that secondary aerosols accounted for 77% of  $\text{PM}_{2.5}$  in Guangzhou during winter 2013, followed by traffic (9%), biomass burning (BB; 7%) and coal combustion (3%). Using the Weather Research and Forecasting/Chem model, Cui et al. (2015) recently found that the most important sources of  $\text{PM}_{2.5}$  in Guangzhou were mobile (37%), industry (32%), power (12%), residential (6.6%), and others (12%, e.g., agriculture, biogenic, airport, and farm machinery) in summer, with respective proportions of 21%, 20%, 2.4%, 4.2%, and 53% in winter. However, in a study based on the CAMx-PSAT source-identification model, only ~10% of  $\text{PM}_{2.5}$  was apportioned to the industry sector in Guangzhou (Wu et al., 2013). Meanwhile, the largest contributor (50%) of  $\text{PM}_1$  was determined to secondary aerosols and BB during 2009–2010 (Tao et al., 2012). Although these model-derived results have been used in attempts to elucidate PM sources in this key megacity, the results are not in good agreement. This is probably in part because the choice of the source categories derived by the models has been defined operationally and in part due to high uncertainties. Sectors such as industry, vehicle, coal combustion, and BB, which can produce large amounts of carbonaceous aerosols, including organic carbon (OC) and elemental carbon (EC), are reportedly the main factors for high uncertainties (50–70%) in the source apportionment of PM using traditional models (Y. Zhang, Huang, et al., 2015; J. Zheng et al., 2009). Therefore, more accurate source identification of OC and EC is urgently needed to reduce this large uncertainty and better guide air pollution control policies and climate change predictions.

Radiocarbon ( $^{14}\text{C}$ , half-life = 5,730 years) is a state-of-the-art tracer that can directly and clearly separate OC and EC into fossil (e.g., coal and petroleum) and nonfossil (e.g., BB and biogenic emissions) sources based on the fact that the fraction of modern carbon ( $f_m$ ) is very close to 1 in nonfossil materials while the  $f_m$  value in fossil fuels is 0 (Szidat, 2009). There is a growing number of  $^{14}\text{C}$ -based studies in China (Andersson et al., 2015; Chen et al., 2013; W. Fang et al., 2017; Huang et al., 2014; J. Liu et al., 2017; J. Liu, Li et al., 2014; Liu, Li, Liu, et al., 2016; Liu, Li, Vonwiller, et al., 2016; Y. Zhang, Li, et al., 2014; Y. Zhang, Liu, et al., 2014; Y. Zhang, Zheng, et al., 2015); however, the existing studies have focused primarily on one PM size and/or on seasons with severe haze pollution (e.g., winter and spring). In our previous studies conducted in Guangzhou, we performed a source apportionment of carbonaceous aerosols of  $\text{PM}_{2.5}$  particles collected in winter (J. Liu, Li, et al., 2014) and spring (J. Liu, Li, Liu, et al., 2016) using the measurements of  $^{14}\text{C}$ , yet knowledge regarding the  $^{14}\text{C}$ -based identification of emission source is still limited in summer. Therefore, to increase understanding of the characteristics of PM in Guangzhou, we performed a simultaneous sampling campaign of  $\text{PM}_{10}$ ,  $\text{PM}_{2.5}$ , and  $\text{PM}_1$  collected daily at an urban site during summer (June–July) in 2013. The concentrations and composition pattern profiles of water-soluble ions (WSIs), OC, EC, and BB tracers (i.e., anhydrosugars) were thoroughly investigated. In particular, we identified an integrated haze event with clear PM concentration and chemical composition dynamics over time. This process was examined using both  $^{14}\text{C}$  and stable nitrogen isotope ( $^{15}\text{N}$ ) signals, which have been found to be a good tracer for studying the emission sources of atmospheric  $\text{NH}_3$  (Chang, Liu, et al., 2016; Pan et al., 2016) and  $\text{NO}_x$  (Zong et al., 2017). Finally, to estimate the relative contributions of emission sources in carbonaceous aerosols,  $\text{NH}_3$  and  $\text{NO}_x$  were calculated from the isotope data, providing new insight into the formation of summer haze in China.

## 2. Experimental Methods

### 2.1. Sampling Campaign

The sampling site (23.1°N, 113.3°E; Figure 1), located on the roof (~20-m height) of the library building of the Guangzhou Institute of Geochemistry, Chinese Academy of Sciences (GIGCAS), was mainly used to monitor and characterize urban pollutants in Guangzhou, China. Most big cities in the PRD region are located in the southern area around Guangzhou, such as Foshan, Zhongshan, Zhuhai, Shenzhen, Macao, Hong Kong, and Dongguan (Figure 1). Other areas, where many people still live in the countryside, are underdeveloped, with low levels of urbanization and industrialization and are generally regarded as rural/suburban areas. For the sample collection, 24  $\text{PM}_{10}$ ,  $\text{PM}_{2.5}$ , and  $\text{PM}_1$  samples (9:00 a.m. to 9:00 a.m. of the next day) were collected simultaneously on prebaked quartz fiber filters using three independent samplers, that were equipped with  $\text{PM}_{10}$ ,  $\text{PM}_{2.5}$ , and  $\text{PM}_1$  inlets, respectively (XTrust Instruments, Shanghai, China) from 25 June 2013 to 15 July 2013. One  $\text{PM}_{2.5}$  (3 July) and three  $\text{PM}_1$  samples (26 June, 2 July, and 8 July) were missed because of

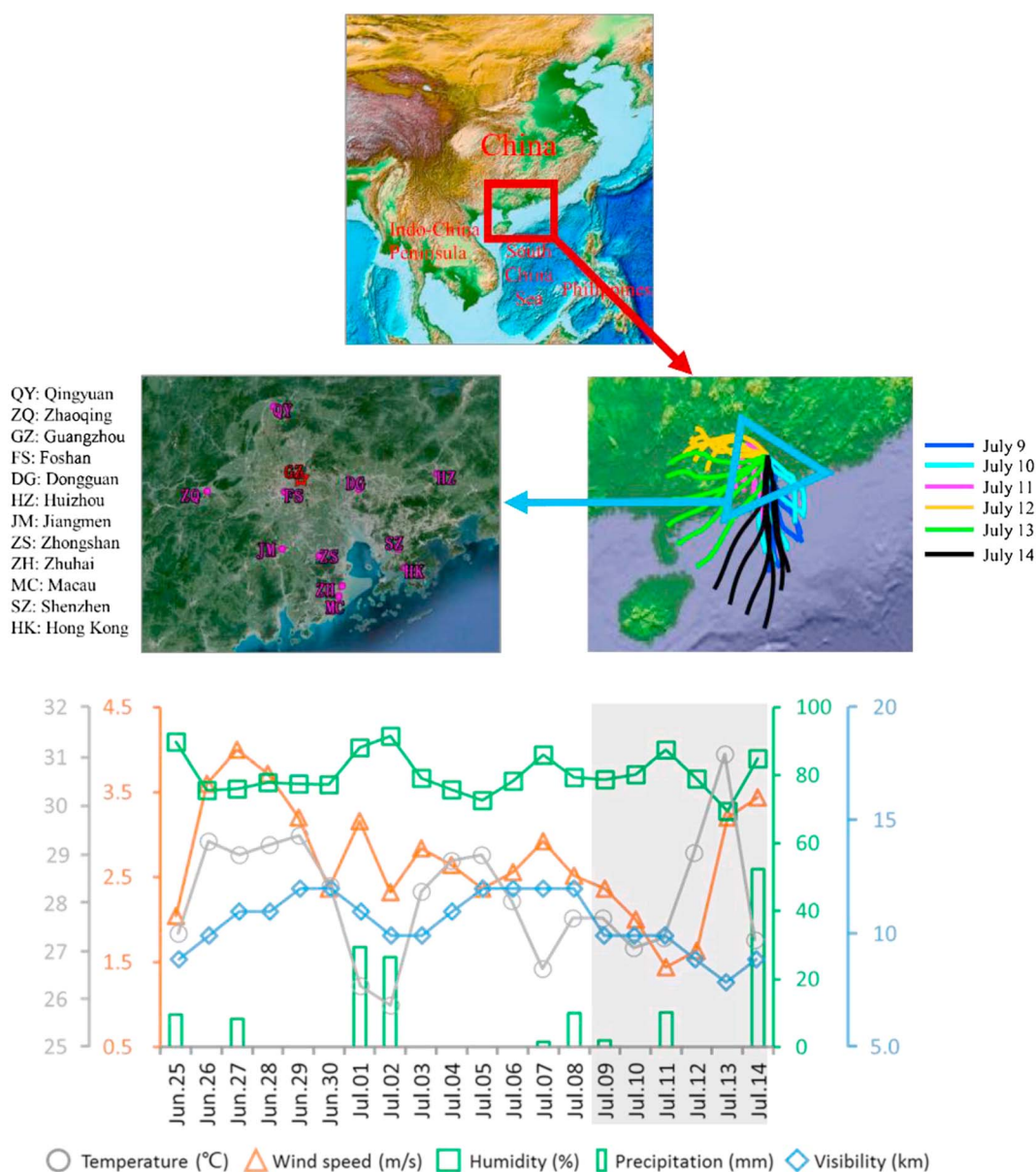


**Figure 1.** Map showing the geographical location of Guangzhou, 24-hr air mass back trajectories and adjacent cities, and meteorological parameters during the sampling time. Back trajectories were modeled every 4 hr at 100 m above ground level during the formation and disappearing of the haze episode of 9–14 July.

instrument failure. Ultimately, we obtained 20  $PM_{10}$ , 19  $PM_{2.5}$ , and 17  $PM_1$  samples. After sampling, all filters and three field blanks were folded in half, wrapped in prebaked aluminum foil, sealed in airtight plastic bags, and stored in a freezer at  $-20^{\circ}\text{C}$  until analysis.

## 2.2. Chemical Analysis

### 2.2.1. Water-Soluble Ions

Filter samples were extracted in ultrapure water (18.2 M $\Omega$ ) with a centrifuge, sonicated in an ice-water bath, and filtered using a Teflon syringe filter (0.22  $\mu\text{m}$ ; Dai et al., 2015). The filtrate was analyzed to quantify eight WSIs (sodium [ $\text{Na}^+$ ], ammonium [ $\text{NH}_4^+$ ], potassium [ $\text{K}^+$ ], magnesium [ $\text{Mg}^{2+}$ ], calcium [ $\text{Ca}^{2+}$ ], sulfate [ $\text{SO}_4^{2-}$ ], nitrate [ $\text{NO}_3^-$ ], and chlorine [ $\text{Cl}^-$ ]) using ion chromatography (883 Basic IC plus, Metrohm, Switzerland).

### 2.2.2. Carbon Species

A piece of filter was cut and sandwiched in a filtration unit equipped with a quartz cartridge and then extracted with ultrapure water slowly and carefully. Our previous results showed that the amount of

extracted water-soluble organic carbon (WSOC) fraction by using this method is almost equal to that soaking for 12 hr in ultrapure water (J. Liu, Li, et al., 2014). The water-extracted filters were subsequently dried in a desiccator. The species of water-insoluble organic carbon (WIOC) and EC were quantified directly from the dried filters using a carbon analyzer (Sunset Laboratory, Inc., United States) at the GIGCAS following the National Institute for Occupational Safety and Health protocol (Birch & Cary, 1996). The difference in total carbon values obtained with and without water-extraction treatment was defined as WSOC species, and OC was defined as the sum of WIOC and WSOC. Noted that a difference (~19%) of WSOC concentration may exist between those indirectly obtained and those directly measured (Hoffer et al., 2006), of which causes are not well understood.

### 2.2.3. Anhydrosugars

Anhydrosugars (galactosan [Gal], mannosan [Mann], and levoglucosan [Lev]) are good tracers of BB and were determined with gas chromatograph-mass spectrometry (GC-MS; Agilent 7890-5975) with a capillary column (DB-5MS, 30 m, 0.25 mm, and 0.25  $\mu$ m; J. Liu, Li, et al., 2014). Before running the GC-MS, samples on filters were spiked with 500 ng of methyl- $\beta$ -L-xylanopyranoside as internal standards, extracted with methanol, reduced using a rotary evaporator, filtered through a Teflon syringe filter, dried in a gentle stream of pure nitrogen gas, and reacted with a 40- $\mu$ l mixture of N,O-bis(trimethylsilyl)trifluoroacetamide (1% trimethylsilyl chloride) and pyridine at 70  $^{\circ}$ C for 1 hr.

### 2.2.4. $^{14}$ C Measurement

The  $^{14}$ C signals of WIOC and EC were determined using a MIni radioCARbon DAting System that equipped with a gas ionizer at the University of Bern, Switzerland (Sizdat et al., 2014), following the Swiss\_4S protocol (Y. Zhang et al., 2012). The obtained WSOC filtrate was frozen at  $-20^{\circ}$ C at GIGCAS, completely freeze-dried in a freeze dryer, transferred into quartz tubes, combusted at 850  $^{\circ}$ C, and reduced to graphite at 600  $^{\circ}$ C using zinc with an iron catalyst (J. Liu, Li, et al., 2014). The isotopic ratios in WSOC were determined using a compact accelerator mass spectrometer (National Electrostatics Corp.) at Peking University, Beijing, China. All  $^{14}$ C results were expressed as  $f_m$ . The  $f_m$  values of the WIOC in samples were corrected based on the  $f_m$  values of the field blanks ( $f_m = 0.62 \pm 0.02$ ). It should be noted that the OC  $f_m$  values in this study were calculated based on the isotopic mass balance. To eliminate the effect of nuclear bomb tests, all  $f_m$  values were converted into the fraction of contemporary carbon ( $f_c$ ) via conversion factors, which were 1.06 for OC and 1.10 for EC for the year 2013 with an uncertainty of 0.05 (J. Liu, Li, et al., 2014). Thus, the relative contributions of fossil  $[(1 - f_c) \times 100\%]$  and nonfossil  $[f_c \times 100\%]$  sources in WIOC, WSOC, OC, and EC could be directly calculated based on their corresponding  $f_c$  values (Table S1 in the supporting information).

### 2.2.5. $^{15}$ N Measurement

Both  $\text{NH}_4^+$  and  $\text{NO}_3^-$  must be converted into  $\text{N}_2\text{O}$  for  $^{15}\text{N}$  measurements with different chemical reaction pathways. Briefly,  $\text{NH}_4^+$  extract was oxidized to nitrite ( $\text{NO}_2^-$ ) using hypobromite ( $\text{BrO}^-$ ), and then converted into  $\text{N}_2\text{O}$  under acidic conditions.  $\text{NO}_3^-$  extract was initially reduced to  $\text{NO}_2^-$  with cadmium power and then reduced  $\text{N}_2\text{O}$  with sodium azide in an acetic acid buffer. Details of these procedures have been published previously (Pan et al., 2016; Zong et al., 2017). The determination of  $^{15}\text{N}_2\text{O}$  was conducted with an isotope ratio mass spectrometer (MAT253, Thermo Fisher Scientific, Waltham, MA, United States) and the  $\delta^{15}\text{N}$  values of the samples relative to the standards were reported as follows:

$$\delta^{15}\text{N} (\text{‰}) = \left[ \left( \frac{^{15}\text{N}/^{14}\text{N}}{^{15}\text{N}/^{14}\text{N}} \right)_{\text{sample}} / \left( \frac{^{15}\text{N}/^{14}\text{N}}{^{15}\text{N}/^{14}\text{N}} \right)_{\text{standard}} - 1 \right] \times 1,000$$

The reference standards used were IAEA- $\text{NO}_3$ , USGS32, USGS34, and USGS35 with an analytical precision of  $<0.3\text{‰}$ . The  $\delta^{15}\text{N}$ - $\text{NH}_3$  values were calculated according to the following equation:

$$\delta^{15}\text{N} - \text{NH}_3 = \delta^{15}\text{N} - \text{NH}_4^+ - \varepsilon\text{NH}_4^+ - \text{NH}_3 \times (1 - f)$$

Here  $\delta^{15}\text{N}$ - $\text{NH}_3$  and  $\delta^{15}\text{N}$ - $\text{NH}_4^+$  represent the  $\delta^{15}\text{N}$  values of  $\text{NH}_3$  and  $\text{NH}_4^+$ , respectively.  $\varepsilon\text{NH}_4^+ - \text{NH}_3$  denotes the corresponding isotope enrichment factor, which is estimated as  $+33\text{‰}$  (Pan et al., 2016). The  $f$  value is the fraction of the initial  $\text{NH}_3$  converted to the ion phase. Since we did not measure daily  $\text{NH}_3$  in this study, the  $f$  values were calculated from simulated  $\text{NH}_3$  and  $\text{NH}_4^+$  using the Weather Research and Forecasting/Chem model (Cui et al., 2015). The model-derived  $f$  values were in the range 0.1–0.5, which are reasonable and similar to previous field studies conducted in summer (~0.2; Lioa et al., 2014). Then,  $\text{NH}_3$  source apportionment was performed with IsoSource, an isotopic mixing model developed by the United States Environmental



**Table 1**  
Summary Statistics of the Concentration ( $\mu\text{g}/\text{m}^3$ ) of Measured Particulate Matters

Particulate matter (PM) type	Minimum	Maximum	Average	Std. Dev
PM <sub>10</sub>	65.4	181	109	28.4
PM <sub>2.5</sub>	41.2	104	57.7	15.0
PM <sub>1</sub>	37.2	93.3	50.9	13.2
PM <sub>2.5</sub> /PM <sub>10</sub>	0.39	0.75	0.55	0.10
PM <sub>1</sub> /PM <sub>2.5</sub>	0.76	0.95	0.88	0.05

Protection Agency (<https://www.epa.gov/eco-research/stable-isotope-mixing-models-estimating-source-proportions>). It should be noted that there are many sources for  $\text{NH}_3$  in the real atmosphere; therefore, the IsoSource model cannot provide a single relative contribution for a given emission source but instead offers feasible solutions. It is necessary to fix the main  $\text{NH}_3$  emission sources before running IsoSource. A recent emission inventory study performed by Pan et al. (2015) found that the main contributors to ambient  $\text{NH}_3$  in the PRD region were fertilizer and livestock, waste, BB, vehicle

exhaust, and coal combustion. To obtain a better comparison with previous  $^{15}\text{N}$ -derived  $\text{NH}_3$  source apportionments in China, the sources of fertilizer, livestock, waste, BB and fossil fuel (traffic + coal combustion) were considered in the IsoSource model in this study, with corresponding  $\delta^{15}\text{N}$ - $\text{NH}_3$  values of  $-50.0\text{‰}$ ,  $-29.1\text{‰}$ ,  $-37.8\text{‰}$  (Chang, Liu, et al., 2016),  $-20\text{‰}$  (Chang & Ma, 2016), and  $-2.95\text{‰}$  (Pan et al., 2016), respectively. Meanwhile, for the  $\delta^{15}\text{N}$ -derived  $\text{NO}_x$  source apportionment, four main endmembers—coal combustion (13.72‰), traffic exhaust ( $-3.71\text{‰}$ ), BB (1.04‰), and biogenic soil emission ( $-33.77\text{‰}$ )—were considered in a newly developed Bayesian mixing model (Zong et al., 2017).

### 3. Results and Discussions

#### 3.1. General Remarks on PM and Measured Chemicals

##### 3.1.1. PM and WSI

The average PM<sub>10</sub>, PM<sub>2.5</sub>, and PM<sub>1</sub> concentration was  $109 \pm 28.4$ ,  $57.7 \pm 15.0$ , and  $50.9 \pm 13.2 \mu\text{g}/\text{m}^3$ , respectively, with the ratios of  $0.55 \pm 0.10$  and  $0.88 \pm 0.05$  for PM<sub>2.5</sub>/PM<sub>10</sub> and PM<sub>1</sub>/PM<sub>2.5</sub> (Table 1). The average ratios of cation to anion in this study were  $1.02 \pm 0.08$ ,  $1.06 \pm 0.08$ , and  $1.07 \pm 0.05$  for PM<sub>10</sub>, PM<sub>2.5</sub>, and PM<sub>1</sub>, respectively (Figure S1), indicating that the ion species selected for quantification were practically satisfied.  $\text{SO}_4^{2-}$  had the highest concentrations in all PM sizes (Table 2), and its relative contribution in measured ions increased slightly with the decrease of PM size (Figure S2). The average proportions were 46% in PM<sub>10</sub>, 54% in PM<sub>2.5</sub>, and 61% in PM<sub>1</sub> (Figure S2). A similar trend was observed for  $\text{NH}_4^+$ . Meanwhile,  $\text{NO}_3^-$  was more enriched in larger particles: accounting for 19% in PM<sub>10</sub>, 13% in PM<sub>2.5</sub>, and 8% in PM<sub>1</sub>, respectively. The average proportions of other ions were generally below 10%. Both the average  $\text{NO}_3^-/\text{SO}_4^{2-}$  and  $\text{NH}_4^+/\text{SO}_4^{2-}$  ratios were low in PM in this study, for example, in PM<sub>2.5</sub>, they were  $\sim 0.24$ , which was only about 50% of those in cities in North China, such as Beijing ( $\sim 0.50$ ) in summer (R. Zhang et al., 2013) and Guangzhou ( $\sim 0.55$ ) in winter (J. Liu, Li, et al., 2014). Given the higher relative humidity in the south and in summer, this finding partly confirms a recent finding that aerosolized water can serve as a reactor for  $\text{NO}_2$  and  $\text{SO}_2$  to accelerate the formation of  $\text{SO}_4^{2-}$  (Cheng et al., 2016), resulting in lower  $\text{NO}_3^-/\text{SO}_4^{2-}$  and  $\text{NH}_4^+/\text{SO}_4^{2-}$  ratios.

##### 3.1.2. OC and EC

The average OC and EC concentrations were  $13.3 \pm 5.70$  and  $1.77 \pm 0.76 \mu\text{g C}/\text{m}^3$  in PM<sub>10</sub>,  $8.36 \pm 3.72$  and  $1.21 \pm 0.50 \mu\text{g C}/\text{m}^3$  in PM<sub>2.5</sub>, and  $6.83 \pm 3.17$  and  $1.03 \pm 0.44 \mu\text{g C}/\text{m}^3$  in PM<sub>1</sub> (Table 3). These results are within comparable orders of magnitude to the results of Cao et al. (2007), who found that the concentrations of OC and EC in 14 Chinese cities during the summer season were in the ranges of 4.8–27 and 1.4–8.0  $\mu\text{g C}/\text{m}^3$ ,

**Table 2**  
Mass Concentrations ( $\mu\text{g}/\text{m}^3$ ) of Water-Soluble Ions

	PM <sub>10</sub>				PM <sub>2.5</sub>				PM <sub>1</sub>			
	Minimum	Maximum	Average	Std. Dev	Minimum	Maximum	Average	Std. Dev	Minimum	Maximum	Average	Std. Dev
$\text{SO}_4^{2-}$	3.54	25.4	7.48	4.78	2.33	17.9	5.30	3.48	2.37	15.5	5.06	3.09
$\text{NO}_3^-$	1.54	6.90	3.05	1.20	0.67	3.72	1.28	0.70	0.30	1.89	0.63	0.34
$\text{NH}_4^+$	0.50	6.56	1.50	1.32	0.45	5.68	1.29	1.18	0.46	4.93	1.31	1.05
$\text{Cl}^-$	0.29	2.42	1.03	0.61	0.17	0.88	0.34	0.16	0.08	0.32	0.16	0.05
$\text{Ca}^{2+}$	1.03	2.77	1.53	0.39	0.37	1.26	0.81	0.27	0.24	0.80	0.46	0.14
$\text{Na}^+$	0.45	2.04	1.02	0.47	0.20	0.65	0.37	0.12	0.12	0.50	0.28	0.09
$\text{Mg}^{2+}$	0.11	0.34	0.21	0.06	0.04	0.17	0.10	0.03	0.02	0.10	0.04	0.02
$\text{K}^+$	0.27	1.33	0.47	0.24	0.17	1.02	0.33	0.20	0.17	0.88	0.32	0.17

**Table 3**  
Concentrations ( $\mu\text{g C/m}^3$ ) of Different Carbon Species and Their Ratios

	PM <sub>10</sub>				PM <sub>2.5</sub>				PM <sub>1</sub>			
	Minimum	Maximum	Average	Std. Dev	Minimum	Maximum	Average	Std. Dev	Minimum	Maximum	Average	Std. Dev
WIOC	2.67	10.4	4.40	1.86	1.53	5.83	2.43	1.03	1.39	5.52	2.23	1.00
WSOC	4.72	23.6	8.86	4.04	3.45	14.3	5.93	2.75	2.47	10.9	4.61	2.21
OC	7.94	34.0	13.3	5.70	4.98	20.1	8.36	3.72	4.05	16.5	6.83	3.17
EC	1.00	3.71	1.77	0.76	0.68	2.65	1.21	0.50	0.58	2.30	1.03	0.44
TC	8.94	37.8	15.0	6.30	5.86	22.8	9.57	4.06	4.84	18.8	7.86	3.51
WIOC/OC	0.27	0.46	0.33	0.05	0.23	0.40	0.30	0.05	0.27	0.39	0.33	0.04
WSOC/OC	0.54	0.73	0.67	0.05	0.60	0.77	0.70	0.05	0.61	0.73	0.67	0.04
OC/EC	5.12	13.7	7.83	2.03	3.36	16.0	7.33	2.65	4.24	15.9	6.90	2.48

Note. EC = elemental carbon; OC = organic carbon; WIOC = water-soluble organic carbon; WSOC = water-soluble organic carbon. TC = total carbon.

respectively. Few studies have examined OC subfractions, such as WIOC and WSOC. The WIOC concentrations in this study were  $4.40 \pm 1.86 \mu\text{g C/m}^3$  in PM<sub>10</sub>,  $2.43 \pm 1.03 \mu\text{g C/m}^3$  in PM<sub>2.5</sub>, and  $2.23 \pm 1.00 \mu\text{g C/m}^3$  in PM<sub>1</sub>, and the respective WSOC concentrations were  $8.86 \pm 4.04$ ,  $5.93 \pm 2.75$ , and  $4.61 \pm 2.21 \mu\text{g C/m}^3$ . For comparison, WSOC concentrations derived from a particle-into-liquid-sampler summer 2006 were in the range of 0–22  $\mu\text{g C/m}^3$  with a median of 4.1  $\mu\text{g C/m}^3$  in a rural site of Guangzhou (Miyazaki et al., 2009), similar to the PM<sub>1</sub> results but lower than that the PM<sub>10</sub> and PM<sub>2.5</sub> results in this study. In addition, a recent study found that an average PM<sub>2.5</sub> WSOC of  $4.08 \pm 2.01 \mu\text{g C/m}^3$  in Guangzhou in winter, similar to the results of this study, but an elevated WIOC ( $6.69 \pm 3.96 \mu\text{g C/m}^3$ ) was observed in winter (J. Liu, Li, et al., 2014).

The average OC/EC, WIOC/OC, and WSOC/OC ratios were  $7.83 \pm 2.03$ ,  $0.33 \pm 0.05$ , and  $0.67 \pm 0.05$  in PM<sub>10</sub>;  $7.33 \pm 2.65$ ,  $0.30 \pm 0.05$ , and  $0.70 \pm 0.05$  in PM<sub>2.5</sub>; and  $6.90 \pm 2.48$ ,  $0.33 \pm 0.04$ , and  $0.67 \pm 0.04$  in PM<sub>1</sub>, respectively. No obvious differences were found in these ratios among particle sizes. The OC/EC, WIOC/OC, and WSOC/OC ratios in Guangzhou have been reported to be 5.1, 0.6, and 0.4 in winter (J. Liu, Li, et al., 2014) and 3.0, 0.6, and 0.4 in spring (Liu, Li, Liu, et al., 2016), respectively. The relatively high OC/EC and WSOC/OC ratios in this study are reflective of the elevated soluble organic carbon (SOC) fraction in summer. These results are in agreement with a previous finding that the SOC/OC ratios estimated by organic tracers (isoprene, monoterpenes,  $\beta$ -caryophyllene, and aromatics) in the PRD region were as much as 4 times in summer than in fall and winter (Ding et al., 2012).

### 3.1.3. Anhydrosugars

Anhydrosugars were predominated by Lev, with an average contribution of 94% (Table 4). The Lev concentrations in PM<sub>10</sub>, PM<sub>2.5</sub>, and PM<sub>1</sub> were  $87.5 \pm 114$ ,  $53.8 \pm 86.7$ , and  $49.4 \pm 82.6 \text{ ng/m}^3$ , respectively; and the respective concentrations were  $1.78 \pm 2.51$ ,  $0.81 \pm 1.45$ , and  $0.74 \pm 1.31 \text{ ng/m}^3$  for Gal and  $4.54 \pm 6.49$ ,  $2.50 \pm 4.34$ , and  $2.40 \pm 4.20 \text{ ng/m}^3$  for Mann. These results are in the same range as those found in a previous study during the summer season, where the PM<sub>2.5</sub> Lev concentrations in 14 Chinese cities varied from 6.2 to 690  $\text{ng/m}^3$  ( $n = 14$ , June to July 2003), with a median concentration of 45  $\text{ng/m}^3$  (G. Wang, Kawamura, et al., 2006). The average PM<sub>2.5</sub> Lev concentration in Beijing was  $230 \pm 370 \text{ ng/m}^3$  ( $n = 50$ , June to July 2011; Cheng et al., 2013), which was  $\sim 1.5$  and  $\sim 4.3$  times higher than those in Chengdu (average =  $152 \pm 89 \text{ ng/m}^3$ ,  $n = 30$ , July 2011), a megacity in western China (Tao et al., 2014) and Guangzhou (average =  $53.8 \pm 86.7 \text{ ng/m}^3$ ,  $n = 19$ , June to July 2013, this study). Meanwhile, the PM<sub>2.5</sub> Lev concentration in winter was 8.0-fold (average =  $432 \pm 301 \text{ ng/m}^3$ ,  $n = 48$ , November 2012 to January 2013; J. Liu, Li, et al., 2014) higher in this study, strongly suggestive of a distinct seasonality of BB in Guangzhou and surrounding areas. It should be noted that sampling days, severity of BB activity, and the sample numbers measured could affect the levels of Lev concentration in regions; more regular Lev measurements are needed in the future to assess the BB status in China. Overall, Lev concentrations in China are lower in southern cities than northern regions, where biofuel such as corn straw is an important energy source for cooking and heating in rural and suburban areas.

Based on the K<sup>+</sup> and Lev measurements in four source samples (wheat straw, corn straw, pine wood, and poplar wood), a study found that the ratio of Lev/K<sup>+</sup> could be used to distinguish between crop ( $<1$ ) and wood ( $>5$ ) burning (Cheng et al., 2013). The Lev/K<sup>+</sup> ratios in this study were 0.11–0.15 (Table 4), seemingly indicative of crop burning in the PRD region in summer. However, this simple parameter should be

**Table 4***Concentrations (ng/m<sup>3</sup>) and the Relative Composition (%) of Anhydrosugars and the Ratios of Lev-to-OC, Mann-to-Gal, Lev-to-Mann, and Lev-to-K<sup>+</sup>*

	PM <sub>10</sub>				PM <sub>2.5</sub>				PM <sub>1</sub>			
	Minimum	Maximum	Average	Std. Dev	Minimum	Maximum	Average	Std. Dev	Minimum	Maximum	Average	Std. Dev
Gal	0.24	10.4	1.78	2.51	0.16	6.54	0.81	1.45	0.05	5.33	0.74	1.31
Mann	0.53	23.6	4.54	6.49	0.32	18.6	2.50	4.34	0.27	17.5	2.40	4.20
Lev	19.1	491	87.5	114	9.21	346	53.8	86.7	4.84	322	49.4	82.6
Gal (%)	0.57	2.95	1.76	0.82	0.58	2.45	1.51	0.52	0.87	2.16	1.28	0.33
Mann (%)	1.53	6.09	4.24	1.89	1.26	7.03	4.65	1.55	1.91	8.26	4.77	1.44
Lev (%)	88.5	97.9	94.0	2.65	90.9	98.1	93.8	2.00	90.2	97.1	94.1	1.67
Lev/K <sup>+</sup>	0.05	0.37	0.15	0.10	0.04	0.35	0.12	0.09	0.03	0.36	0.11	0.10
Lev/Mann	10.8	64.1	28.8	16.2	12.9	77.7	24.5	15.1	10.9	50.7	22.5	9.0
Mann/Gal	1.44	4.26	2.50	0.62	1.88	6.12	3.17	0.92	1.88	5.86	3.84	1.11
Lev/OC	0.0016	0.0155	0.0055	0.0039	0.0016	0.0177	0.0050	0.0047	0.0011	0.0196	0.0052	0.0052

*Note.* OC = organic carbon.

interpreted with caution when classifying BB smoke in ambient air. First, although K<sup>+</sup> generally can be treated as a good tracer of BB (Duan et al., 2004), this cation is not produced solely by BB activity. For example, the emission factor of K<sup>+</sup> from traffic tunnels in the PRD region was estimated to be 0.06 mg·vehicle<sup>−1</sup>·km<sup>−1</sup>, comparable to that of NO<sub>3</sub><sup>−</sup> (0.10 mg·vehicle<sup>−1</sup>·km<sup>−1</sup>; Dai et al., 2015). In addition, PM emitted from the combustion of fossil fuel has a larger K<sup>+</sup> abundance than BB in some cases (Figure S3). Thus, the Lev/K<sup>+</sup> ratio likely loses its specific source fingerprint in cities with high levels of traffic exhaust and coal burning. Second, the Lev/K<sup>+</sup> ratios in some non-wood biomass are higher than those of wood. Although the Lev/K<sup>+</sup> ratios in wood-burning plumes have been higher than 5 in many case studies (Chen et al., 2013), the combustion of other non-wood biomass, such as some types of grass, can also produce a correspondingly high Lev/K<sup>+</sup> ratios of 10–20 (Iinuma et al., 2007; Sullivan et al., 2008). Moreover, the Lev/K<sup>+</sup> ratio from wood burning is highly dependent on the parts of biomass being burned. For example, the Lev/K<sup>+</sup> in burning leaves of wax myrtle, hickory, and juniper can be lower than 0.5 (Sullivan et al., 2008). In a field study conducted in the Chiang Mai Basin, Thailand, no obvious differences could be found for Lev/K<sup>+</sup> ratios between normal days (0.37–0.49) and days impacted significantly by hardwood burning (0.49–0.56; Tsai et al., 2013). These studies imply that the Lev/K<sup>+</sup> ratio should probably not be regarded as an effective tracer for determine BB smoke types in urban areas.

Joint Lev/Mann and Mann/Gal measurements may offer additional information on the origins of BB smoke. A recent study concluded that typical Lev/Mann values in softwood, hardwood, and agricultural residue were 4.3, 23, and 32, respectively (X. Wang et al., 2015), inferring that Lev/Mann can basically distinguish hardwood and agricultural residues from softwood. Similarly, a study found that the Lev/Mann ratio followed the order from highest to lowest of agricultural residue (28 ± 15) > hardwood (22 ± 9) > softwood (4.8 ± 0.8), while that of Mann/Gal was softwood (5.7 ± 3.1) > hardwood (3.0 ± 1.5) > agricultural residue (0.6 ± 0.3; J. Liu, Li, et al., 2014). In this study, the Lev/Mann and Mann/Gal were 28.8 ± 16.2 and 2.50 ± 0.62 in PM<sub>10</sub>, 24.5 ± 15.1 and 3.17 ± 0.92 in PM<sub>2.5</sub>, and 22.5 ± 9.0 and 3.84 ± 1.11 in PM<sub>1</sub>, respectively, displaying characteristics of hardwood burning. This was in agreement with a recent study by J. Liu, Li, Liu, et al. (2016), who found that the average Mann/Gal ratio in Beijing was lower than 1 in spring, when agricultural burning frequently occurs in North China. Guangzhou and adjacent areas are located in a subtropical zone, where the dominant vegetation is hardwood trees such as mango, litchi, longan, and ceiba. These plants are frequently and widely burned in open-air environments in the suburban and rural regions surrounding Guangzhou. In addition, the sampling time (June–July) was not during the central burning season for agricultural residue in Southeast Asia (Figure S4). Therefore, the BB smoke in Guangzhou during the sampling season was associated mainly with hardwood burning.

### 3.2. Daily Dynamic Process: A Major Air Pollution Event

#### 3.2.1. Changes in PM, Chemicals, and Air Masses

A complete haze episode (9–14 July) was observed in this study (Figures 2 and S5). The episode began on 9 July along with a relatively low PM loading, gradually reached a peak on 12 July, displayed a slight downward trend on 13 July, and decreased to the initial level on 14 July. The PM, WIOC, WSOC, EC, K<sup>+</sup>, NO<sub>3</sub><sup>−</sup>, SO<sub>4</sub><sup>2−</sup>, and

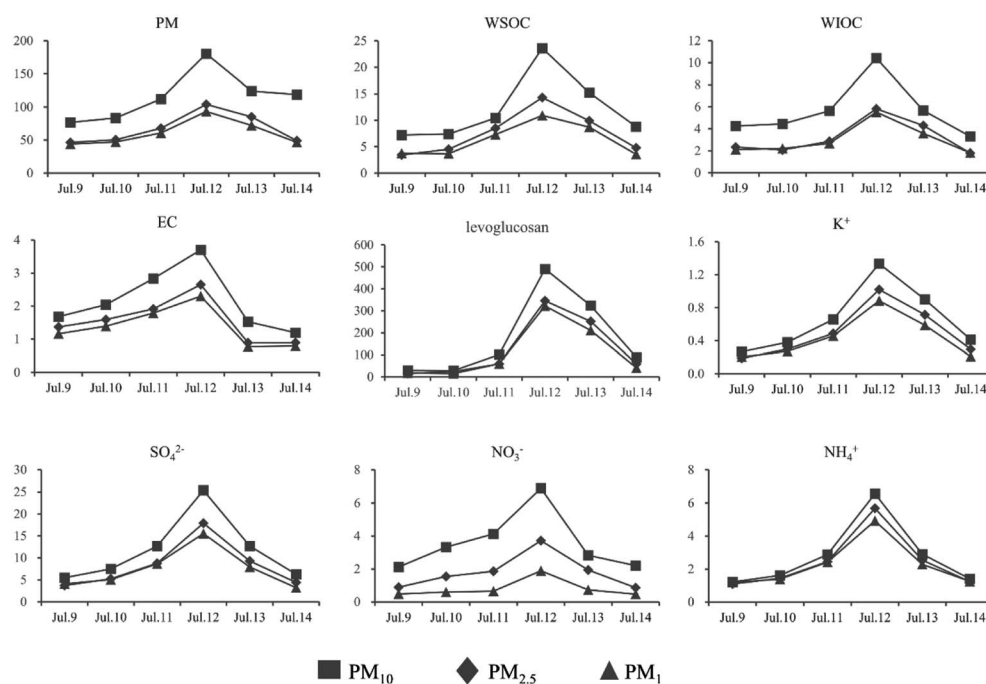


**Figure 2.** Daily dynamics of concentrations for PM ( $\mu\text{g}/\text{m}^3$ ), carbon species ( $\mu\text{g C}/\text{m}^3$ ), levoglucosan ( $\text{ng}/\text{m}^3$ ), and some water-soluble ions ( $\mu\text{g}/\text{m}^3$ ) in Guangzhou during 9 to 14 July. EC = elemental carbon; PM = particulate matter; WSOC = water-soluble organic carbon; WIOC = water-soluble organic carbon.

$\text{NH}_4^+$  loadings on 12 July were 2–5 times higher than those on 9 July. Meanwhile, the Lev concentrations on 12 and 13 July were 15–20 times higher than that on 9 July, which were significantly higher than the concentrations of PM and other chemicals. This demonstrated that a BB plume triggered the growth in PM. Hybrid Single-Particle Lagrangian Integrated Trajectory model (Figure 1) revealed that the origins of the air masses reaching Guangzhou during this episode varied significantly between the areas to the south and west of Guangzhou. During 9–11 July, wind speed gradually decreased from  $\sim 2.5$  to  $\sim 1.5$  m/s, with air masses originating mainly from the South China Sea and passing through southern Guangzhou, which is the main urban and industrial area of the PRD region. Clean marine air diluted the concentrations of PM and other chemicals, leading to relatively good air quality on 9–11 and 14 July. The decrease in wind speed from 9 to 11 July supported the accumulation of local air pollutants from Guangzhou and the southern areas. On 12 July, although the wind speed was as low as that on 11 July, the corresponding air masses were completely free of marine influences and were characterized mainly as originating from western Guangzhou, where there were likely intensive BB activities, because the Lev concentrations were very high on this day. On 13 July, the air mass origin changed to the southwestern area along with a sharp increase in wind speed ( $\sim 3.5$  m/s), which reduced the concentrations of the accumulated air pollutants from the previous days. Finally, the air masses shifted to the southern area on 14 July, and the concentrations of most chemicals returned to original levels on 9 July owing to high wind speeds and strong precipitation.

### 3.2.2. Radiocarbon Results

The daily dynamics of fossil and nonfossil sources during this haze episode are shown in Figure 3. The contributions of fossil sources in all carbon species remained relatively stable during the period 9–11 July, started to drop on 12 July, reached their lowest value on 13 July, and began increasing slightly on 14 July. This phenomenon is explained well by the dynamic variations in air masses reaching the sampling site. Using  $\text{PM}_{2.5}$  as an example, the average proportions of fossil sources in WIOC, WSOC, and EC were  $50 \pm 1\%$ ,  $57 \pm 1\%$ , and  $86 \pm 1\%$ , respectively, from 9 to 11 July, when the air masses originated mainly from the southern area, indicating that the carbon species emitted in Guangzhou had the similar sources to those transported from southern Guangzhou. Given the low marine background levels of PM, these  $^{14}\text{C}$  signals represented mainly local level in the PRD region. On 12 July, when air masses were derived from the western regions, the average proportions of fossil sources in WIOC, WSOC, and EC decreased to  $41 \pm 3\%$ ,  $39 \pm 3\%$ , and  $79 \pm 1\%$ , respectively. These percentage contributions further declined to  $34 \pm 4\%$ ,  $26 \pm 3\%$ , and  $76 \pm 1\%$ , respectively, on



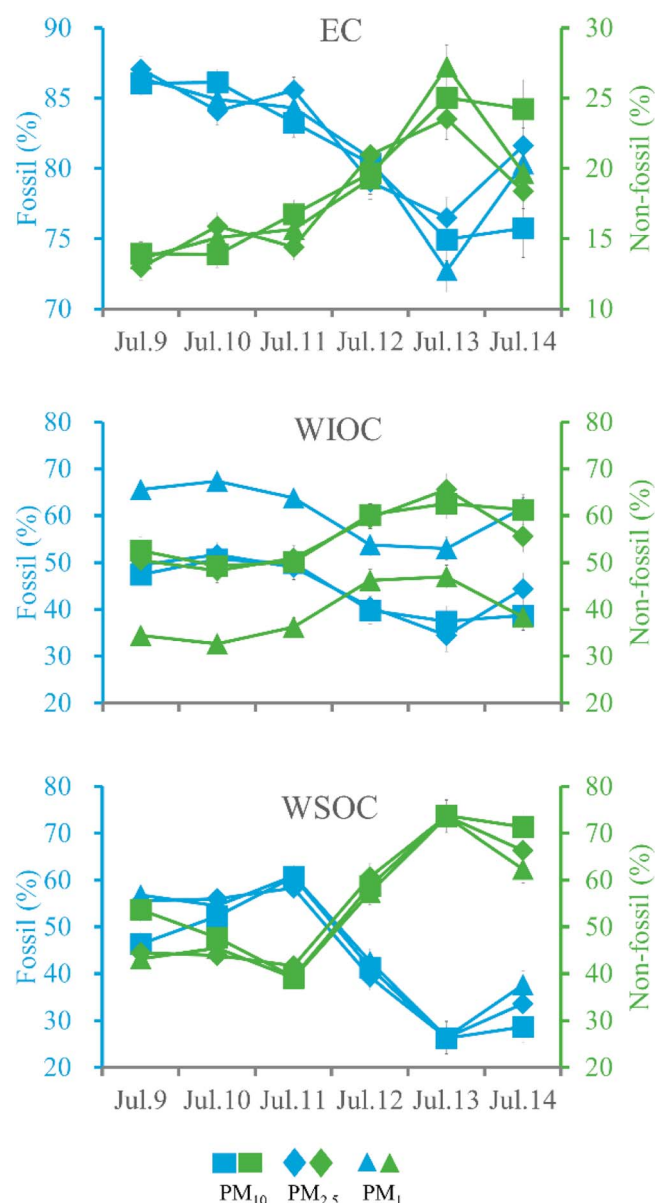


**Figure 3.** Daily dynamics for contributions of fossil and nonfossil sources to EC, WIOC, and WSOC. EC = elemental carbon; PM = particulate matter; WSOC = water-soluble organic carbon; WIOC = water-soluble organic carbon.

13 July when air masses arrived from the southwestern area. These results suggest that carbonaceous aerosols transported from the west or southwest regions such as Zhaoqing, Yunfu, Guangxi Province, and the Indo-China Peninsula via long-range transportation were greatly enriched with  $^{14}\text{C}$  signals compared with those in the PRD region. Finally, the air masses shifted to the southern area again, and the average proportions of fossil sources in WIOC, WSOC, and EC increased slightly to  $44 \pm 3\%$ ,  $34 \pm 3\%$ , and  $82 \pm 1\%$ , respectively. Based on the results of these isotopic signals, differences in air-mass direction determined the source terms of emissions, which had a major influence on air quality in Guangzhou.

Combining all measured samples, the average contributions of fossil sources to WIOC, WSOC, OC, and EC were  $44 \pm 5\%$ ,  $43 \pm 12\%$ ,  $43 \pm 10\%$ , and  $81 \pm 5\%$  in  $\text{PM}_{10}$ ;  $45 \pm 10\%$ ,  $45 \pm 12\%$ ,  $45 \pm 10\%$ , and  $82 \pm 4\%$  in  $\text{PM}_{2.5}$ ; and  $61 \pm 6\%$ ,  $46 \pm 12\%$ ,  $51 \pm 10\%$ , and  $82 \pm 5\%$  in  $\text{PM}_1$ , respectively, with the remainder coming from nonfossil sources (Figure 4). The differences in the fossil contribution to WSOC and EC among the three particle size fractions were very small, indicating that these two carbon species, either from fossil or nonfossil sources, mainly exist in the particle size of  $<1 \mu\text{m}$ . However, the contribution of fossil sources was 30% higher in  $\text{PM}_1$  WIOC than in  $\text{PM}_{2.5}$  and  $\text{PM}_{10}$ , implying that many fossil-related WIOC particles were smaller than those of nonfossil sources. Chen et al. (2013) first investigated the  $^{14}\text{C}$  signals of EC in three Chinese cities, Beijing, Shanghai, and Xiamen, during winter 2009–2010, and found that the fossil source ( $84 \pm 4\%$ ) dominated the origins of EC. In January 2013, Andersson et al. (2015) found that 74%, 68%, and 68% of EC in Beijing, Shanghai, and Guangzhou were associated with incomplete combustion of fossil sources. Y. Zhang, Zheng, et al. (2015) simultaneously reported the  $^{14}\text{C}$  levels of OC and EC in four Chinese cities during winter 2013 and found that the average contributions of fossil sources in OC in Xi'an, Beijing, Shanghai, and Guangzhou were 37%, 58%, 49%, and 35%, respectively, and the corresponding EC values were 78%, 76%, 79%, and 57–80%, respectively. The proportions of fossil sources in WSOC, WIOC, OC, and EC in  $\text{PM}_{2.5}$  in Guangzhou have been reported to be  $33 \pm 3\%$ ,  $40 \pm 6\%$ ,  $37 \pm 4\%$ , and  $71 \pm 10\%$  in winter (J. Liu, Li, et al., 2014) and  $40 \pm 11\%$ ,  $51 \pm 2\%$ ,  $46 \pm 6\%$ , and  $80 \pm 5\%$  in spring (J. Liu, Li, Liu, et al., 2016). Overall, these results suggest several general trends: the contribution of fossil sources in EC in cities are always higher than OC and its subfractions (i.e., WIOC and WSOC); BB exists ubiquitously in all carbon fractions, and its contribution in EC

is sometimes comparable to that in fossil fuel; the  $^{14}\text{C}$  levels of all carbon species can change significantly with changes in the origin of air masses for a given season; and  $^{14}\text{C}$  signals in different carbon species show characteristic seasonality for the sampling site in Guangzhou. The contributions of fossil sources in  $\text{PM}_{2.5}$  ranked from highest to lowest by seasons are summer ( $82 \pm 4\%$ ) > spring ( $80 \pm 5\%$ ) > winter ( $71 \pm 10\%$ ) for EC, summer ( $45 \pm 12\%$ ) > spring ( $40 \pm 11\%$ ) > winter ( $33 \pm 3\%$ ) for WSOC, and spring ( $51 \pm 2\%$ ) > summer ( $45 \pm 10\%$ ) > winter ( $40 \pm 6\%$ ) for WIOC. This shows that summer is the season most impacted by fossil sources in Guangzhou. However, the contributions of fossil sources in all carbon species can decrease significantly with the formation of a haze episode in this season when BB smoke is transported from western areas, exerting major impact on air quality.

### 3.2.3. OC Sources

Figure 5 displays a pie chart of the source apportionment of  $\text{PM}_{2.5}$  OC based on the  $^{14}\text{C}$  and Lev results. In this study, the OC fraction was divided into four parts: fossil WSOC ( $\text{WSOC}_f$ ), fossil WIOC ( $\text{WIOC}_f$ ), OC emitted by BB

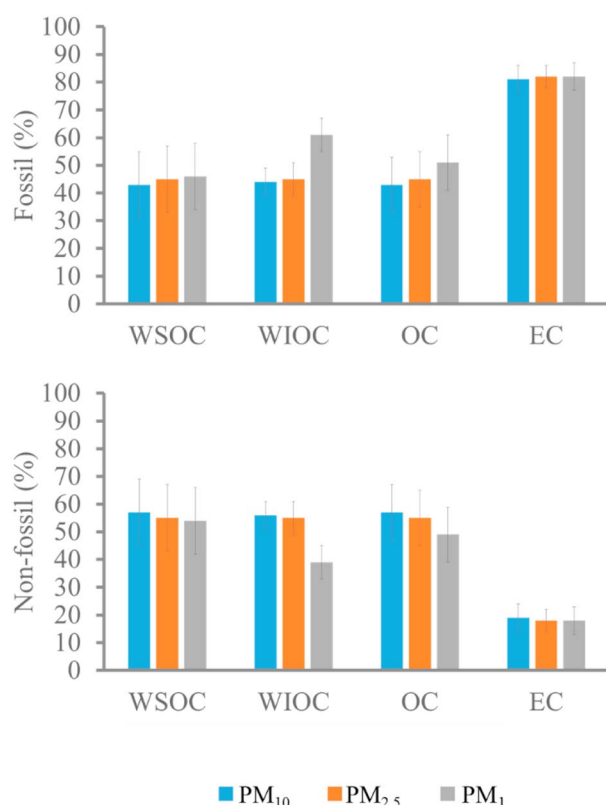


**Figure 4.** Average contributions of fossil and nonfossil sources to WSOC, WIOC, OC, and EC in the summertime of Guangzhou. EC = elemental carbon; OC = organic carbon; PM = particulate matter; WSOC = water-soluble organic carbon; WIOC = water-soluble organic carbon.

(OC<sub>bb</sub>), and the rest of carbon fraction (OC<sub>nbb</sub>), which is calculated from nonfossil OC (OC<sub>nf</sub>) minus OC<sub>bb</sub>. OC<sub>nf</sub>, WSOC<sub>f</sub>, and WIOC<sub>f</sub> were computed directly from their <sup>14</sup>C signals and mass concentrations. OC<sub>bb</sub> was estimated by employing the ratio of OC/Lev ( $7.76 \pm 1.47$ ) of pure hardwood burning (J. Liu, Li, et al., 2014) and the measured Lev concentration. Detailed calculation formulas are available in the supporting information. As expected, OC<sub>bb</sub> contributed a small fraction (2–4%) of OC during 9–11 July, which sharply increased to 13–14% on 12–13 July when Guangzhou was impacted significantly by the air masses from the west and southwest areas. The proportions of WIOC<sub>f</sub> and WSOC<sub>f</sub> in OC were 10–20% and 18–44%, respectively. OC<sub>nbb</sub> was the largest contributor in all samples, ranging from 40% to 58%, consistent with previous findings (J. Liu, Li, Liu, et al., 2016).

PM<sub>2.5</sub> OC<sub>nbb</sub> can be treated as a surrogate of nonfossil secondary organic carbon (SOC<sub>nf</sub>), as the influence of biological carbon (e.g., plant debris) on this particle size is nonsignificant (Guo et al., 2012). Thus, SOC<sub>nf</sub> principally is composed by the OC that formed by the oxidation of biogenic volatile organic compounds and the aging OC of BB. Furthermore, new OC emitted from the combustion of fossil fuel is water insoluble in principle (Weber et al., 2007), and WSOC<sub>f</sub> has been found to be a good proxy for fossil SOC (SOC<sub>f</sub>; J. Liu, Li, et al., 2014; Y. Zhang, Li, et al., 2014). Therefore, WSOC<sub>f</sub> and OC<sub>nbb</sub> were assumed to be the best estimators of SOC<sub>f</sub> and SOC<sub>nf</sub>, respectively, in this study. Consequently, we find that SOC (i.e., WSOC<sub>f</sub> plus OC<sub>nbb</sub>) accounted for 75–84% of OC in this study, which was about 2 to 3 times higher than that in winter (J. Liu, Li, et al., 2014). This estimation is consistent with a model-based study performed by Hu et al. (2010), who reported that the chemical-mass-balance-derived and positive-matrix-factorization-derived SOC contributed 62–82% and

46–89% of OC, respectively, in summer in Hong Kong when it was influenced by air masses from the PRD region. Notably, SOC/OC increased correspondingly with PM<sub>2.5</sub> concentrations during 9–11 July. This indicates that atmospheric reaction is a strong driver in controlling haze formation in urban areas. It should be noted that our results are observed in Guangzhou in one summer season, more unremitting measurements of <sup>14</sup>C for carbon fractions in the future are needed to get a better understanding of the regional conditions of the PRD region for haze pollution.

### 3.2.4. <sup>15</sup>N-Stable Isotope Results

The  $\delta^{15}\text{N-NH}_4^+$  values during the summer haze episode varied significantly, ranging from  $-6.12\text{‰}$  to  $+17.8\text{‰}$  with an average of  $+7.17\text{‰}$  in PM<sub>2.5</sub> (Table 5). These summer values were heavier than those in other heavily polluted cities, such as Beijing during winter 2013 with reported values of  $-37.1\text{‰}$  to  $+5.8\text{‰}$  (Pan et al., 2016) but substantially lighter than rural areas such as Yurijonjo, Japan, ( $+1.3\text{‰}$  to  $+38.5\text{‰}$ ; Kawashima & Kurahashi, 2011) and Gosan, Korea, ( $+4\text{‰}$  to  $+32.2\text{‰}$ ) (Kundu et al., 2010). Given the low correlations between  $\delta^{15}\text{N-NH}_4^+$  and ambient temperature observed in this study ( $R^2 = 0.27$ ), the effect of temperature on the variations in  $\delta^{15}\text{N-NH}_4^+$  signals was probably insignificant compared to the effects of emission sources. In addition, Kundu et al. (2010) also found that temperature correlated poorly with  $\delta^{15}\text{N-NH}_4^+$  signals. Therefore, the large difference in  $\delta^{15}\text{N-NH}_4^+$  signals between Beijing and Guangzhou is largely suggestive of a large difference in emission sources of the precursor gas of  $\text{NH}_4^+$ , that is,  $\text{NH}_3$ , between North and South China. Thus, the dramatic variation in  $\delta^{15}\text{N-NH}_4^+$  signals during this haze event also indicated an invasion of certain sources, as shown by the outcome of the IsoSource model (Figure 6). Almost all  $\text{NH}_3$  (95%) was related to fossil sources on 9 July when the corresponding PM level was relatively low and the air masses originated from southern Guangzhou, underlining the crucial roles of traffic exhaust and coal combustion in ambient  $\text{NH}_3$  generation in urban areas in the PRD region. Notably, the contribution of fossil sources decreased gradually from 10 July (73%) to 13 July (18%) and then increased to 78% on 14 July. In contrast,

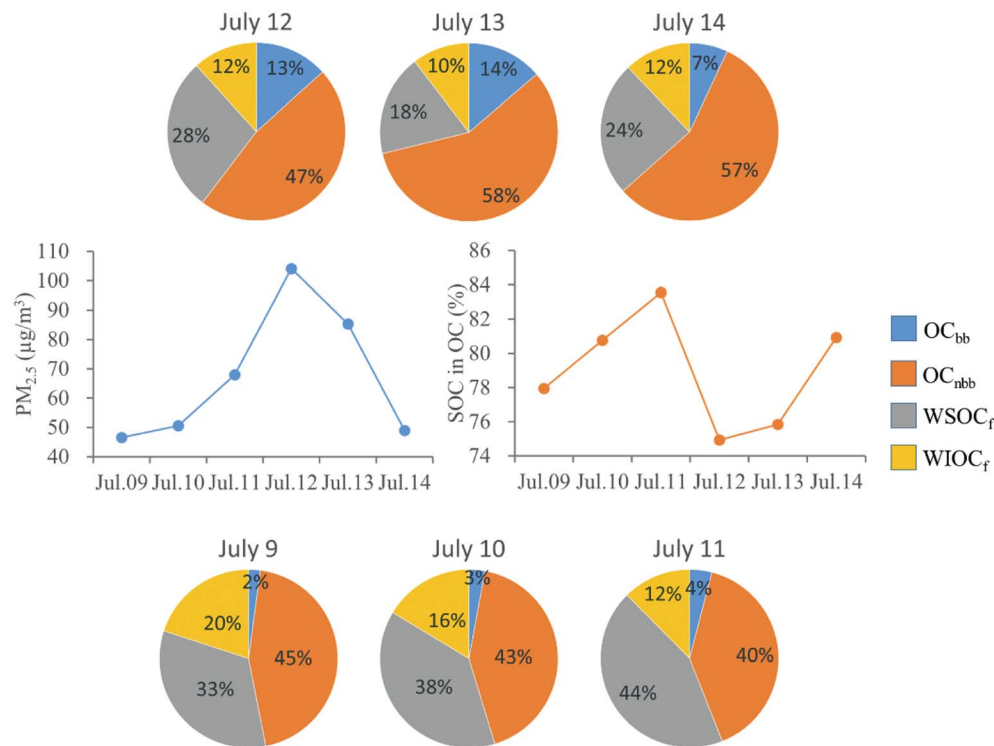


**Figure 5.** Source apportionment of PM<sub>2.5</sub> OC. OC<sub>bb</sub> = organic carbon derived from biomass burning; OC<sub>nbb</sub> = nonfossil organic carbon with the exception of OC<sub>bb</sub>; WSOC<sub>f</sub> = fossil water-soluble organic carbon; WIOC<sub>f</sub> = fossil water-insoluble organic carbon. PM = particulate matter; SOC = secondary organic carbon.

the contributions of emission sources closely related to rural areas showed an obviously increasing trend from 9 to 13 July and then decreased on 14 July. For example, fertilizer sources contributed only 1% of NH<sub>3</sub> on 9 July, up to 14% on 12 July, and 3% on 14 July. This dynamic pattern is largely consistent with that of the <sup>14</sup>C-derived source apportionment, again suggesting that nonfossil sources from the western and southwestern regions of Guangzhou were the key trigger of this summer haze event. Overall, the largest contribution to NH<sub>3</sub> in this study was fossil sources (52 ± 31%), followed by BB (16 ± 10%), livestock (14 ± 9%), waste (10 ± 7%), and fertilizer (8 ± 5%). Fossil sources have generally been thought to be a small contributor to ambient NH<sub>3</sub> based on bottom-up studies in China (Pan et al., 2015; Zhao et al., 2012), while our isotope-based results indicate that these models probably underestimated the importance of these sources, especially those related to traffic exhausts (Chang, Zou, et al., 2016; T. Liu, Wang, et al., 2014).

Compared with the dramatic changes in δ<sup>15</sup>N-NH<sub>4</sub><sup>+</sup>, the δ<sup>15</sup>N-NO<sub>3</sub><sup>-</sup> value showed only slight variations on 9–12 July (+2.59‰ to +5.58‰) and relatively heavier level on 14 July (+9.32‰; Table 5). δ<sup>15</sup>N-NO<sub>3</sub><sup>-</sup> values were reported to be only −4.6‰ to +0.34‰ during summer in a rural site in Japan, probably because of the high activities of bacteria in this season and low emissions from fossil-related combustion (Kawashima & Kurahashi, 2011). In winter, about 2 to 3 times heavier δ<sup>15</sup>N-NO<sub>3</sub><sup>-</sup> values appeared (+2.2‰ to +4.8‰)

due to NO<sub>x</sub> emissions with much heavier δ<sup>15</sup>N signals from the intensive heating based on coal combustion (Kawashima & Kurahashi, 2011). Although similar results have been observed at other northern atmospheric observation sites (Kundu et al., 2010; Zong et al., 2017), this phenomenon was not found in southern cities such as Guangzhou (Y. Fang et al., 2011). This is probably because there is no coal-derived heating in South China in winter, confirming the finding that ambient NO<sub>x</sub> in Guangzhou is dominated by emission sources within the PRD region (Lu et al., 2016).

In this study, the relative contributions of different emission sources in NO<sub>x</sub> basing Bayesian mixing model varied little during 9–14 July

**Table 5**  
δ<sup>15</sup>N Values (‰) of NH<sub>4</sub><sup>+</sup>, NH<sub>3</sub>, and NO<sub>3</sub><sup>-</sup>

Sampling date	δ <sup>15</sup> N-NH <sub>4</sub> <sup>+</sup>	<i>f</i>	δ <sup>15</sup> N-NH <sub>3</sub>	δ <sup>15</sup> N-NO <sub>3</sub> <sup>-</sup>
9 July	+17.83	0.327	−4.38	+2.59
10 July	+12.85	0.297	−10.36	+5.13
11 July	+0.39	0.325	−21.87	+3.67
12 July	−6.12	0.390	−26.27	+5.58
13 July	+2.12	0.124	−26.78	+5.00
14 July	+15.97	0.244	−8.99	+9.32

Note. *f* = fraction of the NH<sub>3</sub> converted to NH<sub>4</sub><sup>+</sup>.

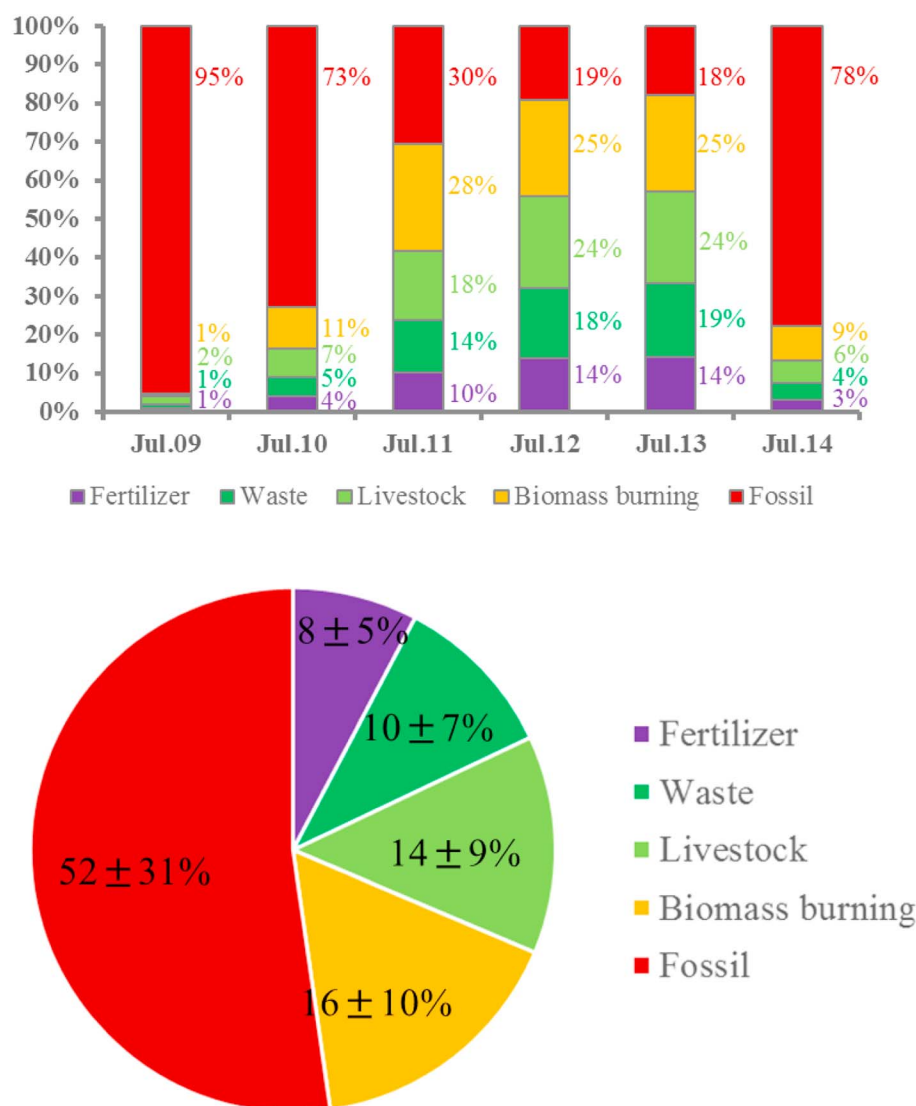


**Figure 6.** Daily source apportionment of Guangzhou NH<sub>3</sub> during 9 to 14 July (up) and the corresponding average values (down).

(Figure S6). On average, coal combustion, BB, vehicle, and biogenic soil contributed  $35 \pm 7$ ,  $29 \pm 1$ ,  $22 \pm 4$ , and  $14 \pm 4\%$  to NO<sub>x</sub> (Figure S6). Noted that this model failed to monitor the pollution invasion from western Guangzhou, and one of the most reasonable explanation is that the large overlaps of <sup>15</sup>N-NO<sub>x</sub> among emission sources, especially those from BB and vehicles (Fibiger & Hastings, 2016). This overlap could result in relatively high uncertainty in estimating the contributions of BB and traffic using Bayesian model (Zong et al., 2017). The relative standard deviation of <sup>15</sup>N-NO<sub>x</sub> signals for BB and mobile sources up to ~400% and ~100% (data were calculated from the supporting information of Zong et al., 2017). Therefore, more source-related measurements of <sup>15</sup>N-NO<sub>x</sub> are urgently needed to improve constraints for source apportionment of NO<sub>x</sub> in future studies.

#### 4. Conclusions

PM<sub>10</sub>, PM<sub>2.5</sub>, and PM<sub>1</sub> in summer 2013 in Guangzhou, the core city of the PRD region, were collected simultaneously in this study. The mass concentrations of PM<sub>10</sub>, PM<sub>2.5</sub>, and PM<sub>1</sub> were 65.4–181, 41.2–104, and 37.2–93.3 μg/m<sup>3</sup>, respectively. The bloom-decay dynamic process of a haze event was monitored in this study, and all PM particles and chemicals measured started to increase from 9 July, peaked on 12 July, and



then decreased gradually to original levels. This air pollution process was the result of changes in meteorological parameters and the inversion of nonfossil sources from western and southern regions of Guangzhou, based on the measurements of Lev,  $^{14}\text{C}$ , and  $^{15}\text{N}$  signals. For instance, the Lev concentrations in  $\text{PM}_{2.5}$  on 12 and 13 July reached 346 and 252  $\text{ng}/\text{m}^3$ , which were significantly higher than that on 9 July (16  $\text{ng}/\text{m}^3$ ), suggesting the importance of BB on this haze-formation process. All  $^{14}\text{C}$  signals were lighter on 13 July when the contributions of nonfossil sources to WSOC, WIOC, and EC were  $74 \pm 3\%$ ,  $66 \pm 4\%$  and  $24 \pm 1\%$ , respectively, while the respective values were  $44 \pm 2\%$ ,  $50 \pm 4\%$ , and  $13 \pm 1\%$  on 9 July. The  $\delta^{15}\text{N}$ -derived model showed that fertilization, waste, livestock, and BB together contributed to 82% of  $\text{NH}_3$  on 13 July but only about 5% on 9 July. However, we did not find obvious changes in  $\text{NO}_x$  sources during the haze event, probably due to the large overlap in  $\delta^{15}\text{N}$ - $\text{NO}_x$  values of BB and traffic exhaust.

This study confirms that the invasion of nonfossil sources from rural and suburban areas to the west and southwest of Guangzhou was the main trigger of the occurrence of a summer haze event in 2013 in the PRD region. In addition, our results highlight the importance of BB in ambient  $\text{NH}_3$  concentration, which is currently underestimated by models and should be considered in greater depth to mitigate large-scale air pollution in China effectively.

### Acknowledgments

We are grateful for financial support from the Natural Science Foundation of China (41430645, 41473101, 41603096, and 91644215), the Guangzhou Science and Technology Program Key Projects (201504010002), and the State Key Laboratory of Organic Geochemistry (SKLOGA201603A). The authors gratefully acknowledge the NOAA Air Resources Laboratory for the provision of the HYSPLIT transport and dispersion model. The authors comply with AGU's data policy, and the data of this work are available at [https://pan.baidu.com/s/1-wZjUDLMceEF\\_1TcocE5\\_w](https://pan.baidu.com/s/1-wZjUDLMceEF_1TcocE5_w). We would like to thank the anonymous reviewers who provided constructive reviews of this manuscript. This is contribution IS-2531 from GIGCAS.

### References

- Andersson, A., Deng, J., Du, K., Zheng, M., Yan, C., Sködl, M., & Gustafsson, Ö. (2015). Regionally-varying combustion sources of the January 2013 severe haze events over eastern China. *Environmental Science & Technology*, 49(4), 2038–2043. <https://doi.org/10.1021/es503855e>
- Birch, M., & Cary, R. (1996). Elemental carbon-based method for monitoring occupational exposures to particulate diesel exhaust. *Aerosol Science and Technology*, 25(3), 221–241. <https://doi.org/10.1080/02786829608965393>
- Cao, J., Lee, S., Chow, J., Watson, J., Ho, K., Zhang, R., et al. (2007). Spatial and seasonal distributions of carbonaceous aerosols over China. *Journal of Geophysical Research*, 112, D22S11. <https://doi.org/10.1029/2006JD008205>
- Cao, J., Lee, S., Ho, K., Zou, S., Fung, K., Li, Y., et al. (2004). Spatial and seasonal variations of atmospheric organic carbon and elemental carbon in Pearl River Delta region, China. *Atmospheric Environment*, 38(27), 4447–4456. <https://doi.org/10.1016/j.atmosenv.2004.05.016>
- Chang, Y., Liu, X., Deng, C., Dore, A., & Zhuang, G. (2016). Source apportionment of atmospheric ammonia before, during, and after the 2014 APEC summit in Beijing using stable nitrogen isotope signatures. *Atmospheric Chemistry and Physics*, 16(18), 11,635–11,647. <https://doi.org/10.5194/acp-16-11635-2016>
- Chang, Y., & Ma, H. (2016). Comment on “Fossil fuel combustion-related emissions dominate atmospheric ammonia sources during severe haze episodes: Evidence from  $^{15}\text{N}$ -stable isotope in size-resolved aerosol ammonium”. *Environmental Science & Technology*, 50(19), 10,765–10,766. <https://doi.org/10.1021/acs.est.6b03458>
- Chang, Y., Zou, Z., Deng, C., Huang, K., Collett, J., Lin, J., & Zhuang, G. (2016). The importance of vehicle emissions as a source of atmospheric ammonia in the megacity of Shanghai. *Atmospheric Chemistry and Physics*, 16(5), 3577–3594. <https://doi.org/10.5194/acp-16-3577-2016>
- Chen, B., Andersson, A., Lee, M., Kirillova, E., Xiao, Q., Kruså, M., et al. (2013). Source forensics of black carbon aerosols from China. *Environmental Science & Technology*, 47(16), 9102–9108. <https://doi.org/10.1021/es401599r>
- Cheng, Y., Engling, G., He, K., Duan, F., Ma, Y., Du, Z., et al. (2013). Biomass burning contribution to Beijing aerosol. *Atmospheric Chemistry and Physics*, 13(15), 7765–7781. <https://doi.org/10.5194/acp-13-7765-2013>
- Cheng, Y., Zheng, G., Wei, C., Mu, Q., Zheng, B., Wang, Z., et al. (2016). Reactive nitrogen chemistry in aerosol water as a source of sulfate during haze events in China. *Science Advances*, 2(12), e1601530. <https://doi.org/10.1126/sciadv.1601530>
- Cui, H., Chen, W., Dai, W., Liu, H., Wang, X., & He, K. (2015). Source apportionment of  $\text{PM}_{2.5}$  in Guangzhou combining observation data analysis and chemical transport model simulation. *Atmospheric Environment*, 116, 262–271. <https://doi.org/10.1016/j.atmosenv.2015.06.054>
- Dai, S., Bi, X., Chan, L., He, J., Wang, B., Wang, X., et al. (2015). Chemical and stable carbon isotopic composition of  $\text{PM}_{2.5}$  from on-road vehicle emissions in the PRD region and implications for vehicle emission control policy. *Atmospheric Chemistry and Physics*, 15(6), 3097–3108. <https://doi.org/10.5194/acp-15-3097-2015>
- Ding, X., Wang, X., Gao, B., Fu, X., He, Q., Zhao, X., et al. (2012). Tracer-based estimation of secondary organic carbon in the Pearl River Delta, south China. *Journal of Geophysical Research*, 117, D05313. <https://doi.org/10.1029/2011JD016596>
- Duan, F., Liu, X., Yu, T., & Cachier, H. (2004). Identification and estimate of biomass burning contribution to the urban aerosol organic carbon concentrations in Beijing. *Atmospheric Environment*, 38(9), 1275–1282. <https://doi.org/10.1016/j.atmosenv.2003.11.037>
- Fan, J., Rosenfeld, D., Yang, Y., Zhao, C., Leung, L., & Li, Z. (2015). Substantial contribution of anthropogenic air pollution to catastrophic floods in Southwest China. *Geophysical Research Letters*, 42, 6060–6075. <https://doi.org/10.1002/2015GL064479>
- Fang, W., Andersson, A., Zheng, M., Lee, M., Holmstrand, H., Kim, S., et al. (2017). Divergent evolution of carbonaceous aerosols during dispersal of east Asian haze. *Scientific Reports*, 7(1), 10422. <https://doi.org/10.1038/s41598-017-10766-4>
- Fang, Y., Koba, K., Wang, X., Wen, D., Li, J., Takebayashi, Y., et al. (2011). Anthropogenic imprints on nitrogen and oxygen isotopic composition of precipitation nitrate in a nitrogen-polluted city in southern China. *Atmospheric Chemistry and Physics*, 11(3), 1313–1325. <https://doi.org/10.5194/acp-11-1313-2011>
- Fibiger, D., & Hastings, M. (2016). First measurements of the nitrogen isotopic composition of  $\text{NO}_x$  from biomass burning. *Environmental Science & Technology*, 50(21), 11,569–11,574. <https://doi.org/10.1021/acs.est.6b03510>
- Guo, S., Hu, M., Guo, Q., Zhang, X., Zheng, M., Zheng, J., et al. (2012). Primary sources and secondary formation of organic aerosols in Beijing, China. *Environmental Science & Technology*, 46(18), 9846–9853. <https://doi.org/10.1021/es2042564>
- Guo, S., Hu, M., Zamora, M., Peng, J., Shang, D., Zheng, J., et al. (2014). Elucidating severe urban haze formation in China. *Proceedings of the National Academy of Sciences of the United States of America*, 111(49), 17,373–17,378. <https://doi.org/10.1073/pnas.1419604111>
- Han, L., Zhou, W., & Li, W. (2016). Fine particulate ( $\text{PM}_{2.5}$ ) dynamics during rapid urbanization in Beijing, 1973–2013. *Scientific Reports*, 6(1), 23604. <https://doi.org/10.1038/srep23604>



- Hoffer, A., Gelencsér, A., Blazsó, M., Guyon, P., Artaxo, P., & Andreae, M. (2006). Diel and seasonal variations in the chemical composition of biomass burning aerosol. *Atmospheric Chemistry and Physics*, 6(11), 3505–3515. <https://doi.org/10.5194/acp-6-3505-2006>
- Hu, D., Bian, Q., Lau, A., & Yu, J. (2010). Source apportioning of primary and secondary organic carbon in summer PM<sub>2.5</sub> in Hong Kong using positive matrix factorization of secondary and primary organic tracer data. *Journal of Geophysical Research*, 115, D16204. <https://doi.org/10.1029/2009JD012498>
- Huang, R., Zhang, Y., Bozzetti, C., Ho, K., Cao, J., Han, Y., et al. (2014). High secondary aerosol contribution to particulate pollution during haze events in China. *Nature*, 514(7521), 218–222. <https://doi.org/10.1038/nature13774>
- Iinuma, Y., Brüggemann, E., Gnauk, T., Müller, K., Andreae, M., Helas, G., et al. (2007). Source characterization of biomass burning particles: The combustion of selected European conifers, African hardwood, savanna grass, and German and Indonesian peat. *Journal of Geophysical Research*, 112, D08209. <https://doi.org/10.1029/2006JD007120>
- Kawashima, H., & Kurahashi, T. (2011). Inorganic ion and nitrogen isotopic compositions of atmospheric aerosols at Yurihonjo, Japan: Implications for nitrogen sources. *Atmospheric Environment*, 45(35), 6309–6316. <https://doi.org/10.1016/j.atmosenv.2011.08.057>
- Kundu, S., Kawamura, K., & Lee, M. (2010). Seasonal variation of the concentrations of nitrogenous species and their nitrogen isotopic ratios in aerosols at Gosan, Jeju Island: Implications for atmospheric processing and source changes. *Journal of Geophysical Research*, 115, D20305. <https://doi.org/10.1029/2009JD013323>
- Lelieveld, J., Evans, J., Fnais, M., Giannadaki, D., & Pozzer, A. (2015). The contribution of outdoor air pollution sources to premature mortality on a global scale. *Nature*, 525(7569), 367–371. <https://doi.org/10.1038/nature15371>
- Lioa, B., Wu, D., Wang, Y., Lin, Y., Wang, S., & Li, F. (2014). Characteristics of particulate SO<sub>4</sub><sup>2-</sup>, NO<sub>3</sub><sup>-</sup>, NH<sub>4</sub><sup>+</sup> and related gaseous pollutants in Guangzhou (in Chinese). *Acta Scientiae Circumstantiae*, 34, 1551–1559.
- Liu, J., Li, J., Ding, P., Zhang, Y., Liu, D., Shen, C., & Zhang, G. (2017). Optimizing isolation protocol of organic carbon and elemental carbon for <sup>14</sup>C analysis using fine particulate samples. *Atmospheric Environment*, 154, 9–19. <https://doi.org/10.1016/j.atmosenv.2017.01.027>
- Liu, J., Li, J., Liu, D., Ding, P., Shen, C., Mo, Y., et al. (2016). Source apportionment and dynamic changes of carbonaceous aerosols during the haze bloom-decay process in China based on radiocarbon and organic molecular tracers. *Atmospheric Chemistry and Physics*, 16(5), 2985–2996. <https://doi.org/10.5194/acp-16-2985-2016>
- Liu, J., Li, J., Vonwiller, M., Liu, D., Cheng, H., Shen, K., et al. (2016). The importance of non-fossil sources in carbonaceous aerosols in a megacity of Central China during the 2013 winter haze episode: A source apportionment constrained by radiocarbon and organic tracers. *Atmospheric Environment*, 144, 60–68. <https://doi.org/10.1016/j.atmosenv.2016.08.068>
- Liu, J., Li, J., Zhang, Y., Liu, D., Ding, P., Shen, C., et al. (2014). Source apportionment using radiocarbon and organic tracers for PM<sub>2.5</sub> carbonaceous aerosols in Guangzhou, South China: Contrasting local-and regional-scale haze events. *Environmental Science & Technology*, 48(20), 12,002–12,011. <https://doi.org/10.1021/es503102w>
- Liu, T., Wang, X., Wang, B., Ding, X., Deng, W., Lü, S., & Zhang, Y. (2014). Emission factor of ammonia (NH<sub>3</sub>) from on-road vehicles in China: Tunnel tests in urban Guangzhou. *Environmental Research Letters*, 9(6), 064027. <https://doi.org/10.1088/1748-9326/9/6/064027>
- Liu, Y., Zhang, T., Liu, Q., Zhang, R., Sun, Z., & Zhang, M. (2014). Seasonal variation of physical and chemical properties in TSP, PM<sub>10</sub> and PM<sub>2.5</sub> at a roadside site in Beijing and their influence on atmospheric visibility. *Aerosol and Air Quality Research*, 14(3), 954–969.
- Lu, X., Yao, T., Li, Y., Fung, J., & Lau, A. (2016). Source apportionment and health effect of NO<sub>x</sub> over the Pearl River Delta region in southern China. *Atmospheric Environment*, 212, 135–146.
- Menon, S., Hansen, J., Nazarenko, L., & Luo, Y. (2002). Climate effects of black carbon aerosols in China and India. *Science*, 297(5590), 2250–2253. <https://doi.org/10.1126/science.1075159>
- Miyazaki, Y., Kondo, Y., Shiraiwa, M., Takegawa, N., Miyakawa, T., Han, S., et al. (2009). Chemical characterization of water-soluble organic carbon aerosols at a rural site in the Pearl River Delta, China, in the summer of 2006. *Journal of Geophysical Research*, 114, D14208. <https://doi.org/10.1029/2009JD011736>
- Pan, Y., Li, N., Zheng, J., Yin, S., Li, C., Yang, J., et al. (2015). Emission inventory and characteristics of anthropogenic air pollutant sources in Guangdong Province (in Chinese). *Acta Scientiae Circumstantiae*, 35, 2655–2669.
- Pan, Y., Tian, S., Liu, D., Fang, Y., Zhu, X., Zhang, Q., et al. (2016). Fossil fuel combustion-related emissions dominate atmospheric ammonia sources during severe haze episodes: Evidence from <sup>15</sup>N-stable isotope in size-resolved aerosol ammonium. *Environmental Science & Technology*, 50(15), 8049–8056. <https://doi.org/10.1021/acs.est.6b00634>
- Sullivan, A., Holden, A., Patterson, L., McMeeking, G., Kreidenweis, S., Malm, W., et al. (2008). A method for smoke marker measurements and its potential application for determining the contribution of biomass burning from wildfires and prescribed fires to ambient PM<sub>2.5</sub> organic carbon. *Journal of Geophysical Research*, 113, D22302. <https://doi.org/10.1029/2008JD010216>
- Sun, Y., Jiang, Q., Wang, Z., Fu, P., Li, J., Yang, T., & Yin, Y. (2014). Investigation of the sources and evolution processes of severe haze pollution in Beijing in January 2013. *Journal of Geophysical Research: Atmospheres*, 119, 4380–4398. <https://doi.org/10.1002/2014JD021641>
- Sun, Y., Wang, Z., Wild, O., Xu, W., Chen, C., Fu, P., et al. (2016). “APEC blue”: Secondary aerosol reductions from emission controls in Beijing. *Scientific Reports*, 6(1), 20668. <https://doi.org/10.1038/srep20668>
- Szidat, S. (2009). Sources of Asian haze. *Science*, 5913, 470–471.
- Szidat, S., Salazar, G., Vogel, E., Battaglia, M., Wacker, L., Synal, H., & Türlér, A. (2014). <sup>14</sup>C analysis and sample preparation at the new Bern Laboratory for the Analysis of Radiocarbon with AMS (LARA). *Radiocarbon*, 56(561), e566.
- Tao, J., Gao, J., Zhang, L., Zhang, R., Che, H., Zhang, Z., et al. (2014). PM<sub>2.5</sub> pollution in a megacity of Southwest China: Source apportionment and implication. *Atmospheric Chemistry and Physics*, 14, 8679–8699.
- Tao, J., Shen, Z., Zhu, C., Yue, J., Cao, J., Liu, S., et al. (2012). Seasonal variations and chemical characteristics of sub-micrometer particles (PM<sub>1</sub>) in Guangzhou, China. *Atmospheric Research*, 118, 222–231. <https://doi.org/10.1016/j.atmosres.2012.06.025>
- Tsai, Y., Sopajaree, K., Chotraksa, A., Wu, H., & Kuo, S. (2013). Source indicators of biomass burning associated with inorganic salts and carboxylates in dry season ambient aerosol in Chiang Mai Basin, Thailand. *Atmospheric Environment*, 78, 93–104. <https://doi.org/10.1016/j.atmosenv.2012.09.040>
- Wang, G., Kawamura, K., Lee, S., Ho, K., & Cao, J. (2006). Molecular, seasonal, and spatial distributions of organic aerosols from fourteen Chinese cities. *Environmental Science & Technology*, 40(15), 4619–4625. <https://doi.org/10.1021/es060291x>
- Wang, X., Bi, X., Sheng, G., & Fu, J. (2006). Chemical composition and sources of PM<sub>10</sub> and PM<sub>2.5</sub> aerosols in Guangzhou, China. *Environmental Monitoring and Assessment*, 119(1–3), 425–439. <https://doi.org/10.1007/s10661-005-9034-3>
- Wang, X., Ju, F., Han, D., Chen, Q., & Wang, W. (2015). Research progress on the organic tracers of biomass burning in atmospheric aerosols (in Chinese). *Environmental Chemistry*, 34, 1885–1894.
- Weber, R., Sullivan, A., Peltier, R., Russell, A., Yan, B., Zheng, M., et al. (2007). A study of secondary organic aerosol formation in the anthropogenic-influenced southeastern United States. *Journal of Geophysical Research*, 112, D13302. <https://doi.org/10.1029/2007JD008408>

- Wu, D., Fung, J., Yao, T., & Lau, A. (2013). A study of control policy in the Pearl River Delta region by using the particulate matter source apportionment method. *Atmospheric Environment*, 76, 147–161.
- Yan, C., Zheng, M., Sullivan, A., Bosch, C., Desyaterik, Y., Andersson, A., et al. (2015). Chemical characteristics and light-absorbing property of water-soluble organic carbon in Beijing: Biomass burning contributions. *Atmospheric Environment*, 121, 4–12. <https://doi.org/10.1016/j.atmosenv.2015.05.005>
- Yang, H., Chen, J., Wen, J., Tian, H., & Liu, X. (2016). Composition and sources of PM<sub>2.5</sub> around the heating periods of 2013 and 2014 in Beijing: Implications for efficient mitigation measures. *Atmospheric Environment*, 124, 378–386. <https://doi.org/10.1016/j.atmosenv.2015.05.015>
- Zhang, Y., Huang, R., El Haddad, I., Ho, K., Cao, J., Han, Y., et al. (2015). Fossil vs. non-fossil sources of fine carbonaceous aerosols in four Chinese cities during the extreme winter haze episode of 2013. *Atmospheric Chemistry and Physics*, 15(3), 1299–1312. <https://doi.org/10.5194/acp-15-1299-2015>
- Zhang, R., Jing, J., Tao, J., Hsu, S., Wang, G., Cao, J., et al. (2013). Chemical characterization and source apportionment of PM<sub>2.5</sub> in Beijing: Seasonal perspective. *Atmospheric Chemistry and Physics*, 13(14), 7053–7074. <https://doi.org/10.5194/acp-13-7053-2013>
- Zhang, Y., Li, J., Zhang, G., Zotter, P., Huang, R., Tang, J., et al. (2014). Radiocarbon-based source apportionment of carbonaceous aerosols at a regional background site on Hainan Island, South China. *Environmental Science & Technology*, 48(5), 2651–2659. <https://doi.org/10.1021/es4050852>
- Zhang, Y., Liu, J., Salazar, G., Li, J., Zotter, P., Zhang, G., et al. (2014). Micro-scale (μg) radiocarbon analysis of water-soluble organic carbon in aerosol samples. *Atmospheric Environment*, 97, 1–5. <https://doi.org/10.1016/j.atmosenv.2014.07.059>
- Zhang, Y., Perron, N., Ciobanu, V., Zotter, P., Minguillón, M., Wacker, L., et al. (2012). On the isolation of OC and EC and the optimal strategy of radiocarbon-based source apportionment of carbonaceous aerosols. *Atmospheric Chemistry and Physics*, 12(22), 10,841–10,856. <https://doi.org/10.5194/acp-12-10841-2012>
- Zhang, Y., Zheng, M., Cai, J., Yan, C., Hu, Y., Russell, A., et al. (2015). Comparison and overview of PM<sub>2.5</sub> source apportionment methods (in Chinese). *Chinese Science Bulletin*, 60(2), 109–121. <https://doi.org/10.1360/N972014-00975>
- Zhao, B., Wang, P., Ma, J., Zhu, S., Pozzer, A., & Li, W. (2012). A high-resolution emission inventory of primary pollutants for the Huabei region, China. *Atmospheric Chemistry and Physics*, 12(1), 481–501. <https://doi.org/10.5194/acp-12-481-2012>
- Zheng, J., Zhang, L., Che, W., Zheng, Z., & Yin, S. (2009). A highly resolved temporal and spatial air pollutant emission inventory for the Pearl River Delta region, China and its uncertainty assessment. *Atmospheric Environment*, 43(32), 5112–5122. <https://doi.org/10.1016/j.atmosenv.2009.04.060>
- Zheng, M., Salmon, L., Schauer, J., Zeng, L., Kiang, C., Zhang, Y., & Cass, G. (2005). Seasonal trends in PM<sub>2.5</sub> source contributions in Beijing, China. *Atmospheric Environment*, 39(22), 3967–3976. <https://doi.org/10.1016/j.atmosenv.2005.03.036>
- Zong, Z., Wang, X., Tian, C., Chen, Y., Fang, Y., Zhang, F., et al. (2017). First assessment of NO<sub>x</sub> sources at a regional background site in North China using isotopic analysis linked with modelling. *Environmental Science & Technology*, 51(11), 5923–5931. <https://doi.org/10.1021/acs.est.6b06316>